Journal of Coastal Research	10	3	716–731	Fort Lauderdale, Florida	Summer 1994

Cross-Shore Structure of Infragravity Standing Wave Motion and Morphological Adjustment: An Example from Northern Zealand, Denmark

Troels Aagaard, Niels Nielsen and Jørgen Nielsen

Institute of Geography
University of Copenhagen
Oster Voldgade 10
DK-1350 Copenhagen K.
Denmark

ABSTRACT

AAGAARD, T.; NIELSEN, N., AND NIELSEN, J., 1994. Cross-shore structure of infragravity standing wave motion and morphological adjustment: An example from Northern Zealand, Denmark. *Journal of Coastal Research*, 10(3), 716–731. Fort Lauderdale (Florida), ISSN 0749-0208.

A set of eight manometer tubes was deployed across a barred surf zone in Northern Zealand, Denmark in order to resolve the cross-shore structure of infragravity wave motions. During a storm, a single dominant standing infragravity wave was generated. This wave had a frequency similar to waves observed on previous occasions. Nearshore bars migrated 5–10 m landward (bar 1) and seaward (bar 2), respectively, with maximum accretion occurring close to the antinodes of the standing wave. The field data thus support theoretical models for bar formation and adjustment, according to which bars are generated through suspended sediment transport convergence at infragravity standing wave antinodes. The generation of the infragravity waves was investigated using bispectral analysis techniques. It was found that during the peak of the storm, two separate incident wave components transferred energy to the infragravity wave. As the storm waned, the incident wave components became further separated in frequency space. Simultaneously, the standing infragravity wave decayed.

ADDITIONAL INDEX WORDS: *Nearshore bars, edge waves, bispectral analysis.*

INTRODUCTION

Within the past decade, the presence and importance of infragravity standing waves in the surf zone has become clearer. These waves having periods of approximately 20–200 seconds may become important in nearshore surface elevation spectra during storms as their amplitude appears to increase linearly with offshore wave height (GUZA and THORNTON, 1982; AAGAARD, 1990a), and they are capable of dominating oscillatory currents and sediment transport processes in the inner surf and swash zones (BEACH and STERNBERG, 1988, 1991; RUSSELL *et al.*, 1991). The length scales and the stationary cross-shore velocity field associated with the waves have led to the suggestion that they may be responsible for nearshore bar formation and/or migration (*e.g.*, SHORT, 1975; BOWEN, 1980; HOLMAN and BOWEN, 1982; AAGAARD, 1990b; BAUER and GREENWOOD, 1990) as drift velocities in the bottom boundary layer of the waves would tend to transport suspended sediment towards the antinodes of the waveform (CARTER *et al.*, 1973).

These hypotheses have not yet been verified. First of all, most studies suggest that infragravity wave energy in nature is broad-banded (*e.g.*, HOLMAN, 1981; GUZA and THORNTON, 1985; OLTMAN-SHAY and GUZA, 1987). The implications of this is that the infragravity waves do not have a preferred cross-shore length scale. The absence of a well-defined length scale would conceptually prevent the formation of distinct bars. Only few studies, conducted during storm-induced dissipative surf zone conditions, have identified the presence of one, or a few, dominant infragravity wave modes (HOLMAN and BOWEN, 1984; AAGAARD, 1990b; BAUER and GREENWOOD, 1990). Secondly, the spatial scale of the waves requires a large number of instruments to properly sample the wave-induced currents and the associated sediment response. Finally, the net currents associated with the standing infragravity waves occur in the bottom boundary layer and no empirical data exist on the thickness and the characteristics of this layer. Furthermore, drift currents might

93033 received 26 March 1993; accepted in revision 20 October 1993.

be masked and difficult to isolate in the presence of other net currents, *e.g.*, undertow or rips.

A simpler but also more ambiguous way of relating morphological change to standing wave action is to measure the surface elevation structure of the standing waves and correlate it with observed bar migration (*e.g.*, SALLENGER and HOLMAN, 1987). However, this method also requires a fairly large number of instruments deployed in a cross-shore and/or longshore array and only a few studies of this character have been conducted. So far, the only successful attempt to convincingly link a standing wave structure to morphological adjustment was reported by BAUER and GREENWOOD (1990) who measured an onshore bar migration with the bar crest located at a standing edge wave antinode.

In this paper, we report on field measurements of the cross-shore surface elevation structure of standing infragravity waves. The data were collected using an array of eight plastic tubes deployed at systematic intervals between 10–160 m from the shoreline, the transect crossing two longshore bars. During the experiment, an infragravity wave occurred having a frequency similar to the waves observed on earlier occasions (AAGAARD, 1990b). These waves were formerly hypothesized to be edge waves with the frequency and mode number determined by a cut-off mechanism induced by the profile geometry (HUNTLEY, 1976; AAGAARD, 1990b). Using bispectral techniques we investigate whether the appearance of the infragravity wave could have been due to triad interactions with incident waves (BOWEN and GUZA, 1978; ELGAR and GUZA, 1985).

FIELD SITE, METHODS AND DATA ANALYSIS

The field work was conducted at Staengehus on the north coast of Zealand, Denmark (Figure 1) during October–December 1990. The beaches on this stretch of coast are generally narrow and backed by till bluffs. However, this particular beach is situated at the former position of an inlet between Kattegat and a now enclosed lake. The inlet was active during the Holocene transgression about 6,000 BP. Since then, the area has been uplifted by about 5 m and the inlet has been infilled by marine sediments. Therefore, sand is relatively abundant and dunes back the approximately 40 m wide beach. No engineering works exist in the vicinity.

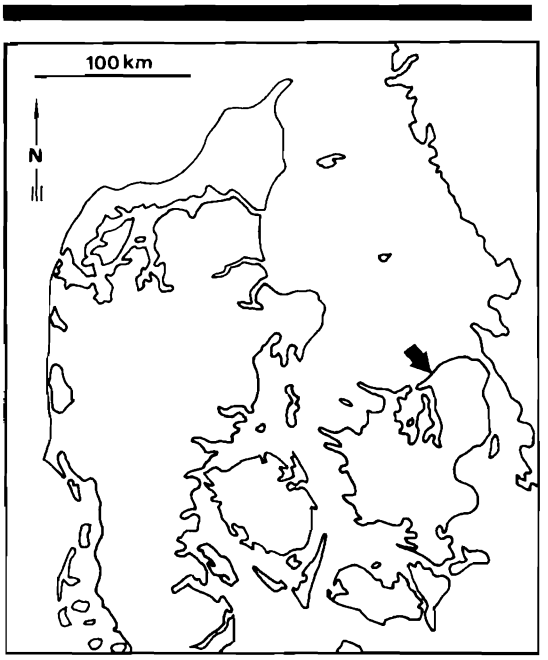

Figure 1. Location of the study area.

The nearshore profile is gently sloping ($\beta \approx 0.015$) with three bars (Figure 2) which are frequently rhythmic alongshore (AAGAARD, 1990b). The mean grain size in the inner surf zone shoreward of x = 200 m is 150–300 μm.

This environment is dominated by long periods of relatively calm conditions interrupted by storm-wave events. Breaker wave heights during onshore storms are typically 2–2.5 m with waves breaking over the third bar, reforming in the trough and a fully saturated inner surf zone between the second bar and the beach. Storm wave periods are generally 5–7 seconds and tides are semidiurnal with a spring range of 0.3 m.

The storm event reported here occurred on November 16–17, 1990. Southwesterly winds veered west and increased to 19 m/sec on November 17, 0300 hr after which the wind slowly decreased to 10 m/sec at 1400 hr. During the evening, the wind backed to the southwest and decreased to 5–7 m/sec. Visually estimated breaker heights over the third bar were approximately 2.2 m on November 17, at 0730 hr, decreasing to around 1.5 m at 1400 hr. Mean longshore currents, measured by an electromagnetic current meter (Marsh McBirney OEM511) and deployed 15 cm above the bottom at x = 100 m, were directed towards

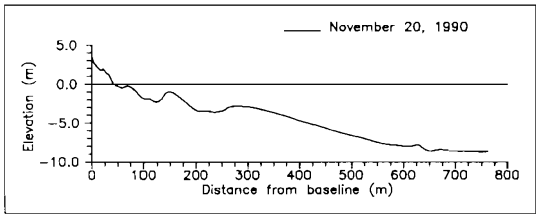

Figure 2. Beach and nearshore profile at Staengehus; November 20, 1990.

the east increasing to 0.63 m/sec on November 17, at 0800 hr. Mean cross-shore currents were directed offshore and peaked at 0.28 m/sec at 0800 hr.

The cross-shore structure of the standing waves was measured using a manometer arrangement modified from the concept of NIELSEN (1988) and NIELSEN *et al.* (1988). Eight transparent PVC tubes, each 200 m in length with an internal diameter (ID) of 10 mm were deployed at x = 52, 61, 73, ≈100, ≈125, ≈150, ≈175 and ≈200 m, respectively (Figure 3). The tubes were numbered T1-T8 with T1 at x = 200 m and T8 at x = 52 m. They were tied to a steel chain and the orifices were covered with filter cloth to reduce the risk of sand intrusion. The tubes were frequently flushed to remove sand grains and air bubbles. At the shoreward end, the PVC tubes were connected to vertical glass tubes having the same ID, fitted with 1-litre reservoir bottles (Figure 4). The tubes were filled with water mixed with $KMnO_4$ to provide a sharp contrast between the water column and the surroundings.

The wave-induced pressure fluctuations in the glass tubes were recorded with a video camera for approximately 20 minutes at two-hour intervals between November 16, 2200 hr and November 17, 1400 hr. The video records were digitized automatically at 4 Hz (AAGAARD and HOLM, 1989), and the time series were truncated to 4,096 data points. These time series were subjected to standard spectral and cross-spectral analyses using the BMDP and SAS statistical analysis packages. Interactions between infragravity and incident waves were determined using bispectral analysis techniques (ELGAR and GUZA, 1985; DOERING and BOWEN, 1986).

It is obvious that the manometer arrangement cannot be used to measure absolute wave heights. Due to viscosity and internal friction in the tubes,

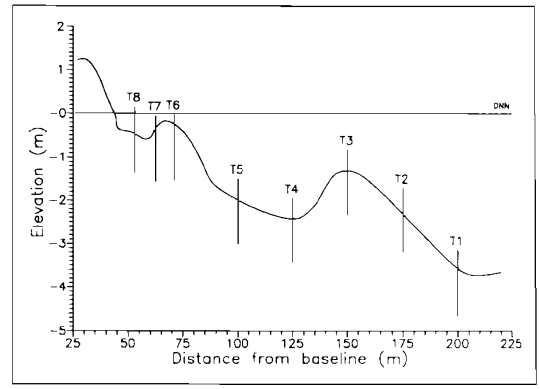

Figure 3. Profile of the inner nearshore region; October 12, 1990. The positions of measurement stations T1-T8 (and DOD-rods) are indicated. DNN = Danish Ordnance Datum.

the system is damped and the response to the pressure fluctuations will be lowered significantly. Furthermore, the gain is frequency dependent. The governing equation for laminar flow in long tubes is

$$\frac{\partial^2 y}{\partial t^2} + \gamma \frac{\partial y}{\partial t} + \omega_0^2 y = \omega_0^2 x \quad . \qquad (1)$$

(NIELSEN, *personal communication*) where γ is a dampening term, depending on the viscosity of the fluid and ω_0 is the resonance frequency of the system = $\sqrt{(g/L)}$, where g is the gravitational acceleration and L is the length of the tube; x and y are input and output, respectively. Assuming $\sqrt{(2\nu/\omega)} \ll r$, with ν being the kinematic viscosity of the fluid, ω the radian frequency of the oscillation and r the radius of the tube, $\gamma = (32\nu/D^2)$ where D is the tube diameter.

However, as mentioned above, the tubes were fitted with reservoir bottles at the landward end. Assuming $ay \ll V_0$, where a is cross-sectional area of the tube and V_0 the volume of the reservoir, Equation 1 is modified to

$$\frac{\partial^2 y}{\partial t^2} + \frac{32\nu}{D^2}\frac{\partial y}{\partial t} + \left[\omega_0^2 + \frac{P_0 a}{\rho L V_0}\right] y = \omega_0^2 x \qquad (2)$$

where P_0 is pressure in the system at rest and ρ is fluid density. Letting $x = \eta\, e^{i\omega t}$ (where η is offshore wave amplitude and ω the angular frequency of the waves) and assuming $y = R\eta\, e^{i\omega t}$, where R is the gain of the system, the frequency response function becomes

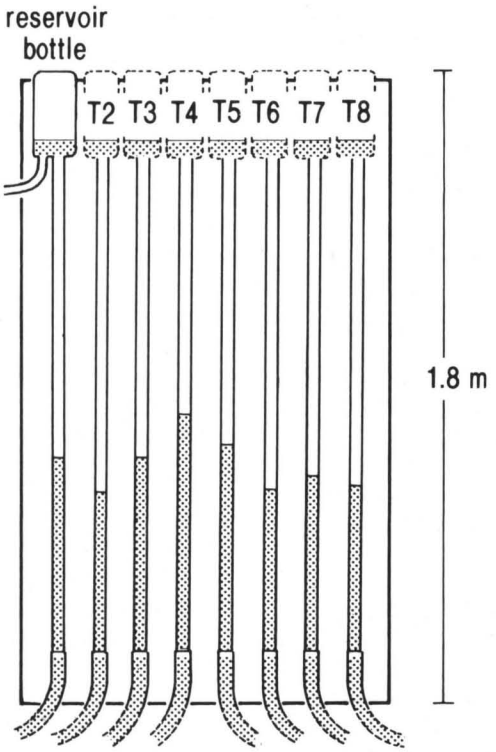

Figure 4. (Top) Schematic representation of the manometer setup on the beach. The vertical glass tubes are each connected to a PVC tube. Reservoir bottles are fitted to each glass tube to provide a negative pressure in order to avoid water draining from the tubes. When the tubes are filled or flushed, an electric pump is fitted to the short length of tube inserted into the reservoir bottles. The water level excursion in the glass tubes is recorded with a video camera. (Bottom) Photo of the manometer. Only three tubes are in operation.

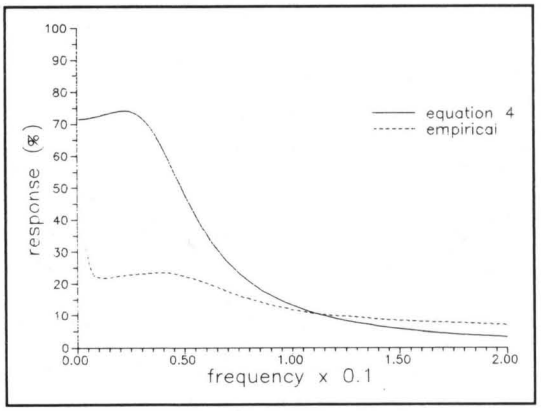

Figure 5. Theoretical and empirical frequency response curves of the manometer as a function of frequency. The empirical curve is based on correlations with a collocated pressure transducer.

$$R(\omega) = \frac{1}{\left(1 + \frac{P_0 a}{\rho L V_0 \omega_0^2}\right) - \left(\frac{\omega}{\omega_0}\right)^2 + i\left(\frac{32\omega\nu}{\omega_0^2 D^2}\right)} \quad (3)$$

Letting $P_0 = 0.5$ atm., and using $L = 200$ m, $D = 0.01$ m, $V_0 = 1$ litre, the amplitude response can be approximated as

$$R(\omega) = \frac{1}{\sqrt{\left(1.4 - \left(\frac{\omega}{0.221}\right)^2\right)^2 + (6.4\omega)^2}} \quad (4)$$

This theoretical frequency response function is plotted in Figure 5, as well as results from empirical calibrations. The empirical frequency response curve was constructed from several shallow water intercomparisons (roughly 1 m water depth) between a 200 m PVC tube and a pressure transducer. It is seen that the empirically determined response at infragravity frequencies is significantly lower than predictions from Equation 4, while response at incident wave frequencies is more or less similar. It is difficult to explain this discrepancy at low frequencies. The friction term in Equation 2 is based on the assumption that the boundary layer in the tubes occupies the entire tube diameter ($\sqrt{(2\theta/\omega)} \ll r$). This assumption is violated for the frequencies of interest here, and the frictional attenuation of the signal will be larger than given by Equation 2. However, this violation should be more critical for the high frequencies which do not seem to be affected. As

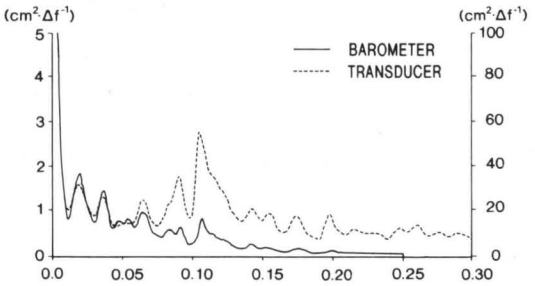

Figure 6. Comparison of spectra from collocated manometer tubes and pressure transducers. The spectra have 38 degrees of freedom. The left-hand vertical scale refers to the spectral variance of the manometer tube, while the one on the right applies to the transducer.

absolute wave heights are not considered in the present study, these discrepancies between theoretical and empirical frequency response do not appear critical. What is more important in this context is that the field tests demonstrated that the spectral structure is correctly reproduced. Figure 6 shows an example of simultaneously recorded spectra from a manometer tube and a pressure transducer.

The fact that the tubes are not rigid might also cause some response to the ambient pressure along the tubes. However, this effect is considered to be of minor importance. The tubes appear to correctly reproduce the spectral structure (*e.g.*, Figure 6) as well as phases (see below), which suggests that tube flexibility is not critical.

Morphological changes were monitored using echo-sounder and standard surveying techniques. Further, eight depth-of-disturbance (DOD) rods (GREENWOOD and HALE, 1980; GREENWOOD and OSBORNE, 1991) were deployed at the manometer stations (Figure 3). The rods measure maximum depth of erosion through determination of the level of a sliding washer relative to the top of the rod. They also record net bed elevation change as the level of the bed is measured before and after the event, again relative to the top of the rod.

RESULTS

Infragravity Waves

Wind and wave parameters through the storm event are shown in Figure 7. Visual observations of breaker height, beginning at first light, suggested that H_b steadily decreased from 0720 hr. The recorded wave data (H_s) shown in Figure 7

were obtained using the current meter in the trough between bars 1 and 2. Wave height was determined using linear theory ($H_s = 4(\langle u^2 \rangle h/g)^{1}$, where $\langle u^2 \rangle$ is the vector sum of the variance in the velocity record, h is water depth and g is gravitational acceleration). The current meter indicates a peak energy level around 1000 hr. However, as H_s appears to trace the water level, the wave height at this location was probably depth limited. The increased water level (+0.7 m Ordnance Datum) was due to a storm surge which is a common phenomenon along the Danish coasts during westerly winds.

As earlier reported by BAUER and GREENWOOD (1990), the growth of the infragravity energy lagged the incident wave energy. In Figure 8, spectra from T2 (x = 175 m) are shown for November 16, 2200 hr and November 17, 0200, 0600, 1000 and 1400 hr. As mentioned above, breaker heights peaked prior to 0720 hr (Figure 7), while the infragravity energy did not reach its maximum level until 1000 hr. It should be mentioned that Figure 8 suggests that incident wave heights also peaked at 1000 hr. However, T2 was well within the surf zone and incident wave heights, therefore, depended on water depth; mean water level increased consistently through the event (Figure 7).

Initially, the infragravity band was dominated by energy around 0.033 Hz (Figure 8). Energy at this frequency persisted throughout most of the storm, but it tended to decay towards the shoreline; and as will be shown below, it did not exhibit a coherent standing wave structure. Around 0200 hr, a spectral peak began to form at around 0.018 Hz (55.5 seconds). This peak grew and became statistically significant (95% -level) at 0600 hr. As shown in Figure 9, energy at this frequency was present across the surf zone. The figure shows the spectra recorded at 0800 hr from T2, T4 and T8. Unfortunately, T6 was buried or clogged throughout the event and no useful data were recorded from this location. The fact that peak frequency was consistent across the surf zone suggests that the spectral peaks were not due to the cross-shore structure of a broadbanded shoreline spectrum. A swash spectrum recorded with the video camera at 0720 hr on November 17 similarly shows infragravity peaks corresponding to those found in the surf zone (Figure 10). During the waning of the storm, energy at 0.018 Hz decreased in relative magnitude (Figure 8).

The 0.018 Hz wave displayed a consistent cross-shore standing wave structure. As shown in Figure 11a, only the band 0.012–0.022 Hz was in accordance with standing wave characteristics (a phase relationship of 0 or $\pm \pi$), and only this band had a statistically significant coherence between stations T2 and T8. However, there is also a coherence peak at 0.036 Hz which is marginally significant. Figure 11b shows cross-shore phase angles determined with respect to T2, for the frequencies 0.018 and 0.033 Hz. It is seen that the 0.018 Hz band exhibited a consistent standing wave structure with significant cross-shore coherence and an 180° phase jump shoreward of T4. As the phase change appeared to occur around T5, it is probable that a surface elevation node was located close to this station. Contrarily, the phase relationships at 0.033 Hz suggest a motion which is progressive towards the shoreline, even though these relationships are only significant at some

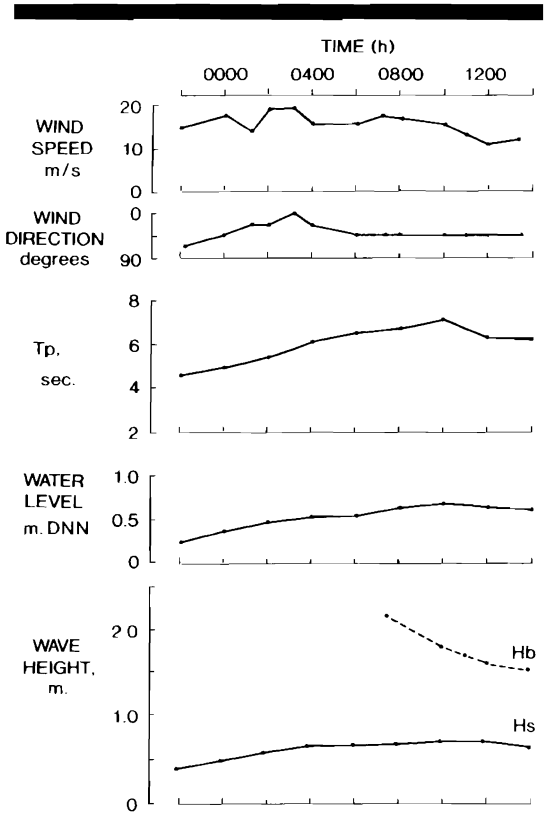

Figure 7. Wind speed and wind direction relative to shore-normal, peak spectral period of the cross-shore current (T_p), water level (DNN = Danish Ordnance Datum), visually estimated breaker height over the third bar (H_b) and significant wave height at the current meter in the trough between bars 1 and 2 (H_s).

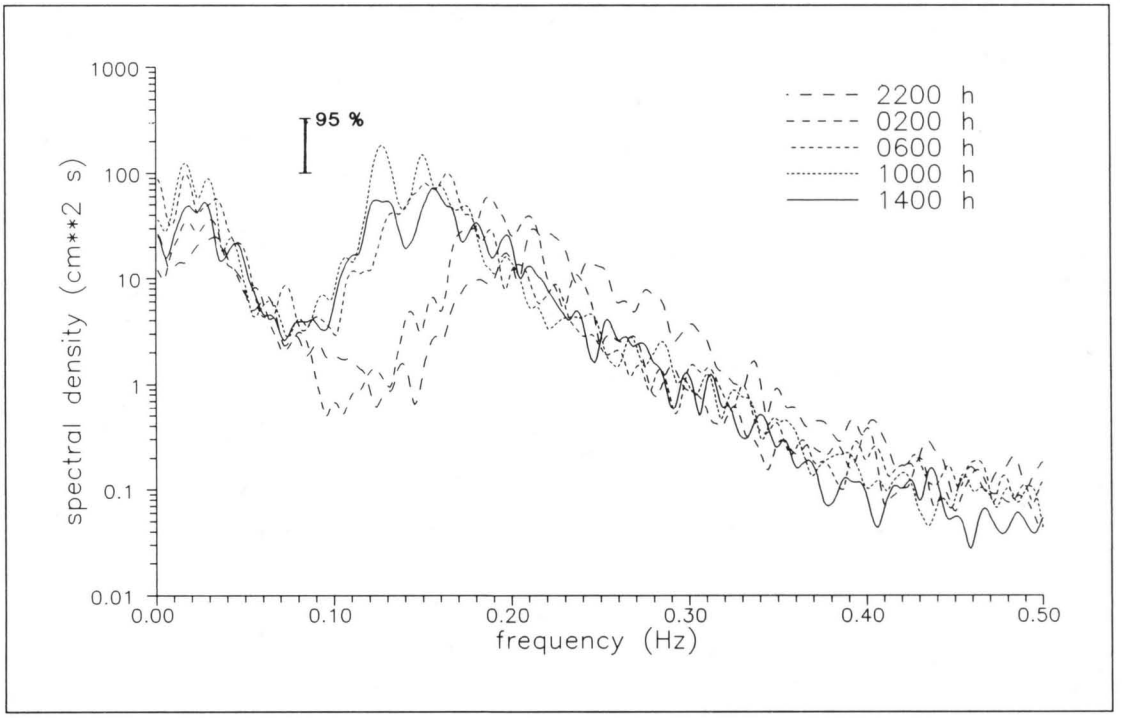

Figure 8. Energy spectra from T2 on November 16, 2200 hr and November 17, 0200, 0600, 1000 and 1400 hr. The spectra have 30 degrees of freedom (df).

locations. It is concluded that while the 0.018 Hz band represents a cross-shore standing wave motion, the 0.033 Hz band shows erratic behaviour and/or progressive incident wave motion.

Also plotted in Figure 11b is the theoretical cross-shore velocity potential for an edge wave having a frequency of 0.018 Hz, and three offshore zero-crossings (n = 3). A slope of $\beta = 0.0150$ determined from the method suggested by HOLMAN and BOWEN (1979) has been used. This method estimates the effective slope for non-linear beach profiles. The edge wave structure has been adjusted horizontally for the observed mean water level at 0600 hr (at x = 23 m). Predicted nodal positions for this edge wave are located between T4 and T5 (x = 116 m) and shoreward of T8 (x = 39 m); antinodes are predicted close to T2 (x = 176 m) and between T6 and T7 (x = 66 m) which is reasonably consistent with the pattern determined in the field. However, the wave could also have been a leaky mode standing wave, as the measurement positions were too widely spaced to resolve the small differences in cross-shore structure between edge waves and leaky modes at this distance from the shoreline. Superimposed on the theoretical edge wave structure in Figure 11b is the measured spectral variance at 0.018 Hz. The variance at T2 has been selected to coincide with the theoretical structure, and the variances at T1 and T3–8 have been plotted relative to T2. It is seen that while there is a reasonably good correspondence between the theoretical and measured variance structure in the outer surf zone, measured variance is too small over the inner bar, especially at T6 (which was clogged and/or buried) and T7. The reason for the rather low response in T7 and T8 may have been due to small air bubbles in the tubes, caused by the intense wave breaking.

Morphological Change

The profile was surveyed on November 8, and again on November 20, the two surveys bracketing the storm event discussed here. Figure 12 shows the results from these surveys, as well as the data from the DOD-rods. The survey data indicate a

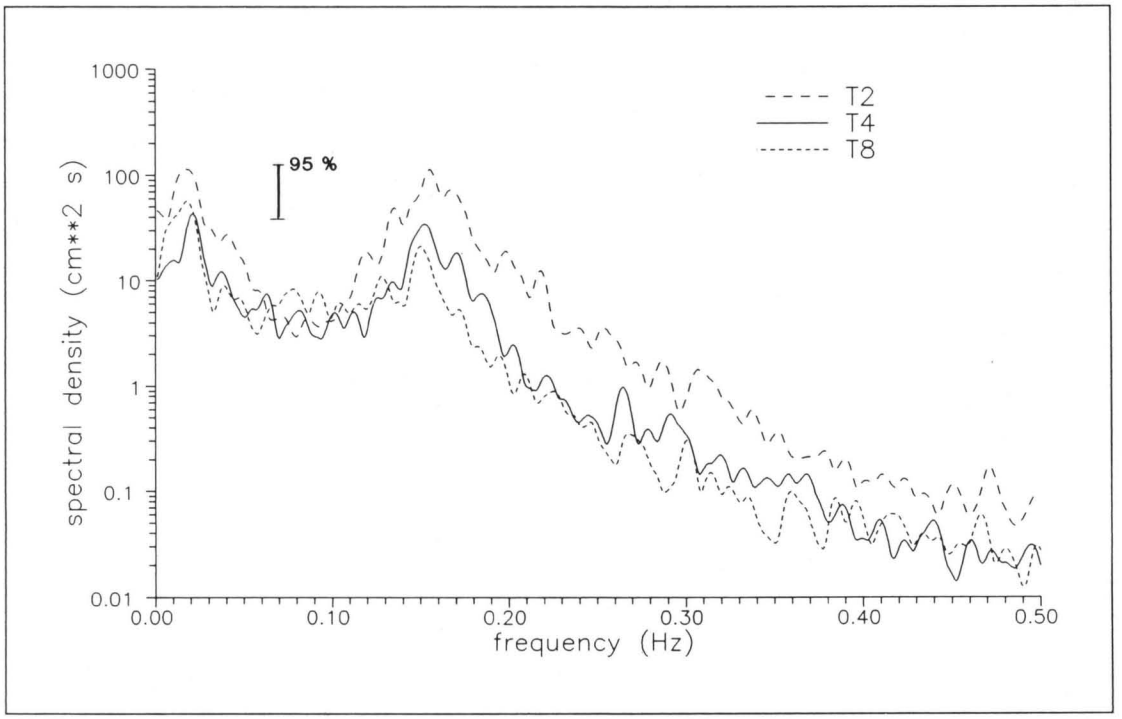

Figure 9. Energy spectra from T2, T4 and T8; November 17, 0800 hr. df = 30.

shoreward migration of the inner bar on the order of 5 m, as well as a seaward migration (5–10 m) of the second bar. The bars also appear to have accreted somewhat, with the accretion mainly taking place close to the computed antinode positions of the standing waves (landward slope of the inner bar; seaward slope of the second bar), even though a localized accretion occurred in the trough close to the second node. The survey data thus suggest an accretion of sediment around standing wave antinodes, which has earlier been reported by BAUER and GREENWOOD (1990). However, the DOD-rods show some discrepancies compared to the surveys. The maximum depth of erosion was in the trough between the bars, or rather at the toe of the second bar (close to the standing wave node), but net bed elevation changes are somewhat different from the surveys. The rod at T6 suggests a net erosion of 0.12 m whereas the survey indicates no significant change in elevation. The rods on the seaward slope of the second bar registered much lower accretion values than the surveys (0.03–0.04 m, compared with approximately 0.20 m). The accretion at the crests of both bars as well as the small accretion in the trough was not detected. The reasons for the discrepancies may be survey errors (the boat slightly off the survey line), and the fact that the positions of the outer DOD-rods were not surveyed exactly, or localized scour around the DOD-rods. In hindsight, the number of DOD-rods should have been increased significantly to properly resolve the bed elevation changes. For example, the accretion on the landward slope of the inner bar is missed completely in the rod data. Nevertheless, in general the surveys and the DOD-rods record the same trends; *i.e.*, erosion on the landward slope and accretion on the seaward slope of the second bar.

Wave-Wave Interactions

The incident wave spectra from the manometer tube at the outer edge of the second bar (T1) often suggested the presence of two separate incident wave peaks (Figure 13). The frequencies of these peaks are shown as a function of time in Figure 14. One of the spectral peaks (solid line in Figure

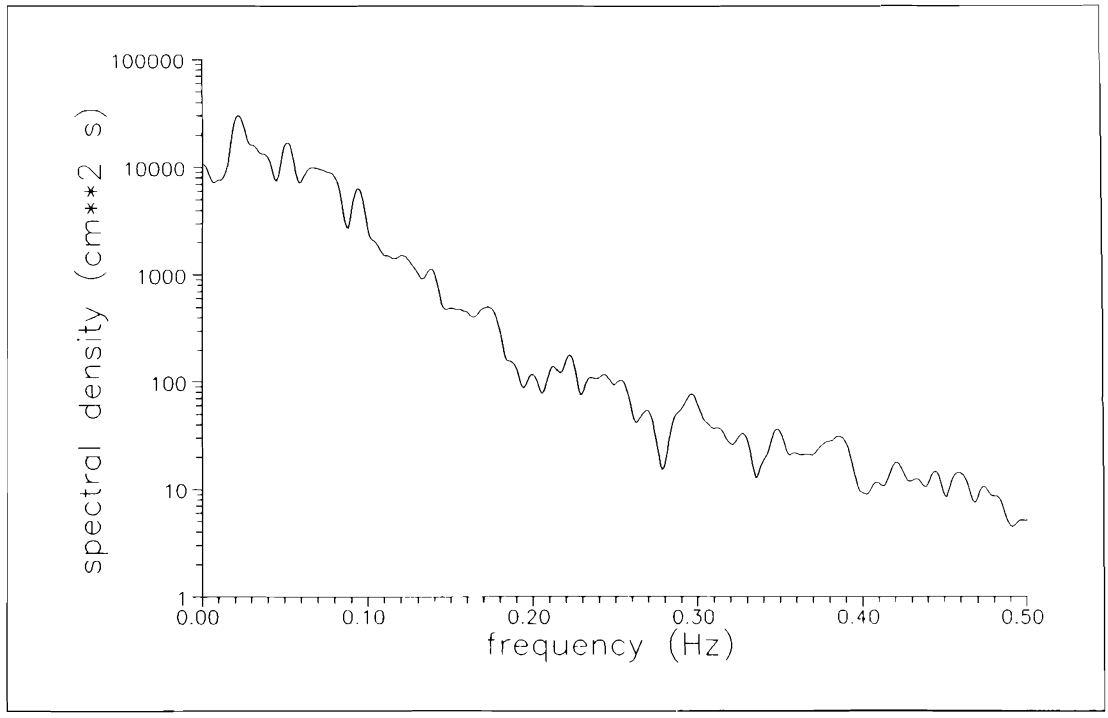

Figure 10. Swash spectrum recorded on November 17, 0720 hr. df = 38.

14) seemed to decrease in frequency until 0400 hr after which it became rather stable at a frequency of approximately 0.155 Hz. A second peak (dashed line in Figure 14) appeared in the spectra from 0200 hr at a somewhat higher frequency (see also Figure 13). However, the spectral composition changed significantly at around 1000 hr and lower frequencies became more prominent.

Infragravity waves are probably generated through difference interactions in the incident wave band, according to

$$\omega_1 - \omega_2 = \omega_3 \quad (5)$$

where ω_1, ω_2 are incident wave frequencies, and ω_3 is the infragravity wave frequency (*e.g.*, LONGUET-HIGGINS and STEWART, 1962; BOWEN and GUZA, 1978; ELGAR and GUZA, 1985). In the edge wave case, the relationship becomes somewhat more complicated, as the angle of wave incidence and edge wave dispersion have to be taken into account. Thus, for edge waves, the infragravity (edge) wave frequency becomes

$$\omega_3^2 = \omega_e^2 = |\omega_1^2 \sin \alpha_1 - \omega_2^2 \sin \alpha_2| \sin(2n + 1)\beta \quad (6)$$

(GALLAGHER, 1971; BOWEN and GUZA, 1978), where α_1, α_2 are the incidence angles of two wave trains relative to the shore-normal, n is the edge wave mode number, and β is the nearshore slope. This relationship cannot be directly tested here, as we have no information on the angles of wave incidence.

However, from inspecting Figure 14, it is possible that difference interactions between the two identified incident wave peaks could have generated an infragravity wave. Further, the infragravity response should be approximately constant between 0200 hr and 0800 hr, whereas it should change significantly subsequent to 1000 hr as ($\omega_1 - \omega_2$) became significantly larger. As mentioned above, the 0.018 Hz infragravity wave appeared at 0200 hr and persisted through 1000 hr after which its presence could no longer be established in the records. Using bispectral analysis techniques, it is possible to investigate triad in-

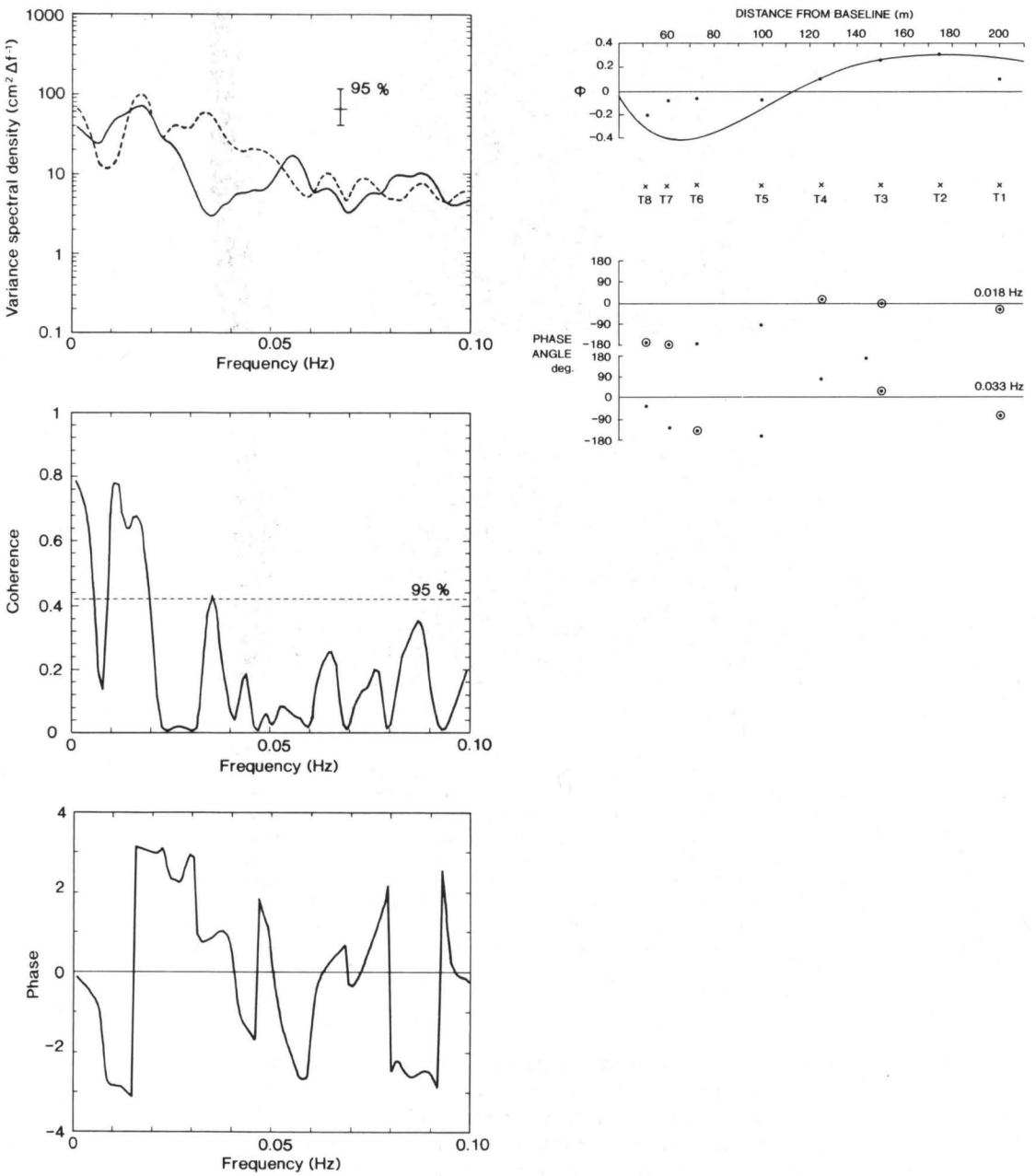

Figure 11. (Left) Cross-spectra of T2 and T8; November 17, 0600 hr. Spectral density (T2 = dashed line; T8 = solid line), coherence and phase are shown. df = 22. (Right) Computed cross-shore structure and relative amplitudes of the 0.018 Hz wave (top), as well as phase angles measured relative to T2 at 0.018 Hz and 0.033 Hz; November 17, 0600 hr. Circled dots in the phase plots are significantly coherent at the 5%-level.

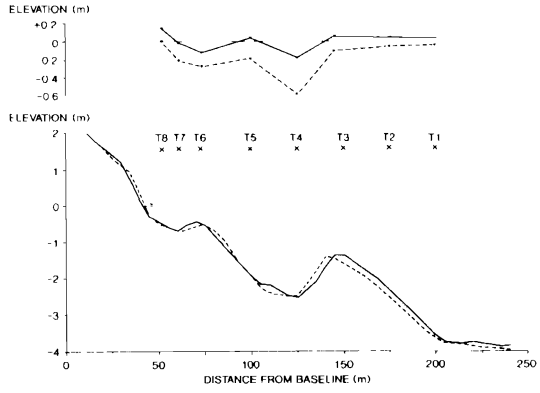

Figure 12. The nearshore profile on November 8 (dashed line) and November 20 (solid line), as well as maximum depth of erosion (dashed line) and net bed elevation change (solid line), measured at the DOD-rods over the same period of time.

teractions (*i.e.*, persistent phase-coupling between three wave frequencies; ELGAR and GUZA, 1985, 1986; DOERING and BOWEN, 1986, 1987) to ascertain whether energy transfers did occur between the incident wave components identified here and the 0.018 Hz wave.

The autobispectrum is given by

$$B(f_1, f_2) = E[A(f_1)A(f_2)A^*(f_1 - f_2)] \quad (7)$$

(KIM and POWERS, 1979), where $A(f_1)$ is the complex Fourier-coefficient of frequency f_1, * denotes the complex conjugate and E[ ] is an expected-value or average operator. If the difference wave f_3 (= $f_1 - f_2$; or the sum wave $f_3 = f_1 + f_2$) is generated through an interaction between f_1 and f_2, the value of B will be non-zero, and a phase-coherence will exist (DOERING, 1988). The strength of the coupling between the wave components is measured through the bicoherence (which is analogous to cross-spectral coherence, but for a three-wave system) which is a normalized version of the bispectrum:

$$b^2(f_1, f_2) = \frac{|B(f_1, f_2)|^2}{E[|A(f_1)A(f_2)|^2]E[|A(f_1 - f_2)|^2]} \quad (8)$$

(KIM and POWERS, 1979). The 95% confidence level for zero bicoherence can be defined as

$$b_{95\%} \approx (6/df)^{1/2} \quad (9)$$

where df is the number of degrees of freedom in the bispectrum (HAUBRICH, 1965). Bicoherence levels indicate the strength of the coupling; they do not, however, provide information regarding

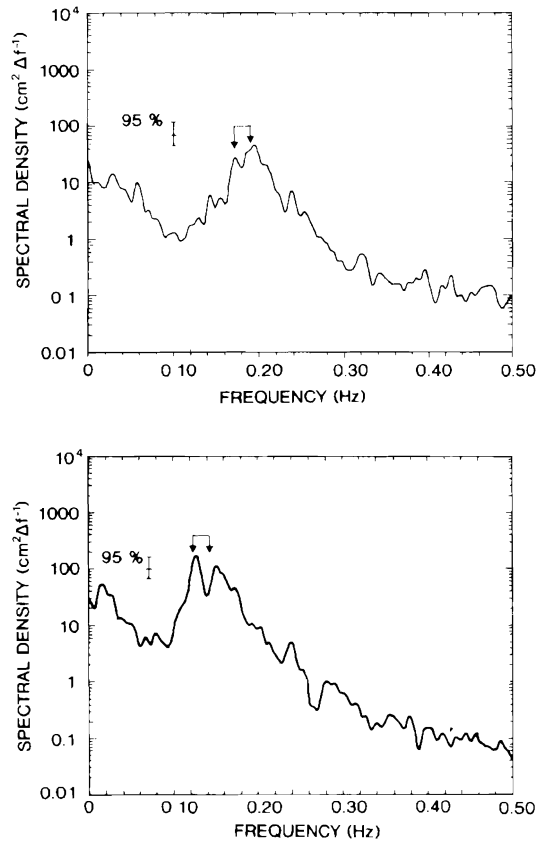

Figure 13. Energy spectra from T1; November 17, 0200 hr (upper diagram) and 1000 hr (lower diagram). df = 30. The most important incident wave frequencies involved in triad interactions with the 0.018 Hz infragravity wave are indicated by arrows.

the relative contributions of a given interaction to the total nonlinearity of the record. The bispectrum ($B(f_1, f_2)$) may be expressed as a biamplitude and a biphase. DOERING and BOWEN (1986) utilized such bispectral amplitudes to isolate the strongest triad interactions in bispectra.

Here, bicoherence and biamplitude levels have been computed to isolate the most significant couplings between the 0.018 Hz wave and incident wave components. Incident wave components simultaneously having maxima in bicoherence and biamplitude were selected. The records from T1 have been used and the 4096 data points were partitioned into four blocks. Bispectral estimates were ensemble-averaged over these four blocks, and bicoherences/biamplitudes were computed

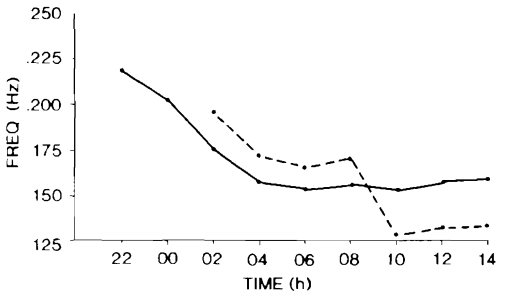

Figure 14. Frequencies of incident wave peaks as identified in the spectra, as a function of time. Initially, only one peak existed (solid line), but from 0200 hr onwards, a secondary incident peak appeared (dashed line). This latter peak was subjected to a significant downshift in frequency at 1000 hr, at the time when the wind forcing of the wave field decreased.

Table 1. *Incident wave frequencies involved in triad interactions with the 0.018 Hz wave (f_1,f_2), and bicoherence levels of these interactions. Bicoherence above 0.52 is significant at the 5% -level. Also shown are the cases when the incident wave frequencies corresponded to the two spectral peaks (+), and the cases when the 0.018 Hz wave was seen in the spectra (+).*

Time (hr)	(f_1,f_2)	Bicoh.	(f_1,f_2) at Inc. Wave Peaks	0.018 Hz
2200	(0.191, 0.211)	0.55	–	
0000	(0.191, 0.211)	0.60		
0200	(0.176, 0.195)	0.60	+	+
	(0.195, 0.211)	0.59	–	
0400	(0.156, 0.172)	0.57	+	+
0600	(0.148, 0.164)	0.69	+	+
0800	(0.133, 0.149)	0.62		+
	(0.148, 0.164)	0.55	+	
1000	(0.145, 0.165)	0.59		+
1200	(0.137, 0.153)	0.59	–	–
	(0.152, 0.168)	0.80	–	
1400	(0.121, 0.141)	0.66		
	(0.145, 0.164)	0.58	–	

using a Fast Fourier Transform. Results were merged over three neighbouring frequency bands, yielding a total of 24 degrees of freedom (df).

In Table 1, the incident wave components identified as having the strongest interactions with the 0.018 Hz wave have been listed, as well as the bicoherence levels of these interactions. All bicoherence values are significant at the 5% -level. Initially, the interactions did not involve two incident wave spectral peaks (se also Figure 14); but at 0200 hr, the appearance of a secondary incident wave component resulted in an interaction involving the two incident wave peaks identified and energy at 0.018 Hz. Interestingly, the 0.018 Hz wave appeared in the energy spectra at this point in time (Figure 8). Interactions involving the two spectral peaks identified in Figure 14 persisted up to and including 0800 hr, subsequent to which there was a substantial frequency shift in the incident wave band and the interactions now only involved one of the incident wave peaks. Figures 13a and b show the spectra from T1 at 0200 and 1000 hr. In the first case, both incident wave peaks were involved in the strongest interaction (shown with arrows on the diagram), while at 1000 hr, the incident wave components were probably separated too far in frequency space to interact with the 0.018 Hz wave. Further, the individual peaks may also have been too narrow to interact with the 0.018 Hz wave. It is perhaps significant that the 0.018 Hz wave disappeared at 1200 hr (Figure 8). Studying Table 1, it appears that a correlation does exist between the cases where the strongest interaction involved both incident wave spectral peaks and the cases where the 0.018 Hz wave occurred. Even though the bispectrum does not reveal the direction of energy flow in triad interactions, it is highly likely that the incident waves transferred energy to the infragravity wave. When the spectral composition changed at 1000 hr, the infragravity wave disappeared, albeit with some time lag (Table 1).

DISCUSSION AND CONCLUSIONS

The data presented here have suggested the occurrence of only one infragravity standing wave mode in the surf zone. Two dominant low-frequency waves were detected in the spectra, one having a frequency of 0.018 Hz, and the other a frequency of approximately 0.033 Hz. However, only the former displayed standing wave characteristics, *i.e.*, a 180° phase jump in the surf zone, whereas the latter had cross-shore phases suggesting progressive incident wave motion. The results, therefore, resemble those reported by BAUER and GREENWOOD (1990) from an extreme storm event on a dissipative beach, characterized by gentle gradients. On that occasion, only a single dominant infragravity wave (shown to be a standing edge wave) was found. In conjunction with reports from high-energy dissipative beaches in Oregon (HOLMAN and BOWEN, 1984; BEACH and STERNBERG, 1991), it does appear that significant amounts of incident wave dissipation are needed

Table 2. *Phase relations at 0.018 Hz, between cross-shore and longshore velocity at T5.*

Time (hr)	Phase Angle (degrees)	Coherence
2200	144	0.29
0000	93	0.28
0200	104	0.30
0400	7	0.62*
0600	152	0.71*
0800	176	0.48*
1000	180	0.62*
1200	89	0.24
1400	52	0.38

Note: * indicates significant coherence at the 5% level

in order to promote the occurrence of one dominant infragravity standing wave mode.

Other things being equal, the occurrence of one dominant standing wave mode should enhance the possibility of infragravity waves being important in the processes of nearshore bar migration and ultimate positioning. During the experiment reported here, the first and second bars experienced onshore and offshore migration, respectively, on the order of 5–10 m. Given the magnitude and duration of the event (approximately 18 hr), the morphological adjustment was not very substantial. This illustrates the stability and permanency of nearshore bar systems along shorelines dominated by fetch-restricted storm wave events (*e.g.*, GREENWOOD, 1986; AAGAARD, 1988; DAVIDSON-ARNOTT and MCDONALD, 1989).

After the event, the bars were located close to observed positions of surface elevation antinodes. Whether the infragravity waves were in fact instrumental in the adjustment of the bars cannot be ascertained given the absence of data on bottom currents and sediment transport. All that can be said is that the documented response was in accordance with theoretical predictions (*i.e.*, bars moving to antinode positions due to transport of suspended sediment; *e.g.*, CARTER *et al.*, 1973; BOWEN, 1980; HOLMAN and BOWEN, 1982). Undertow models for bar formation and migration (*e.g.*, SVENDSEN, 1984; DALLY, 1987) cannot be ruled out, however. During the storm peak, the surf zone was saturated with respect to incident waves. Under such conditions, the undertow model predicts offshore bar migration exclusively, accretion of the breakpoint bar and erosion of the inner bar, the latter not being in accordance with the field observations. However, during conditions of decreasing wave heights towards the end of the storm, waves started reforming in the trough between the first and second bars and a renewed breaking over the first bar could have caused a renewed accretion of this bar. It is possible, therefore, that undertow was a contributing factor to the bar migration.

However, the results obtained here support the conclusions and hypotheses reported by AAGAARD (1990b), who used data recorded previously at the same beach. On those occasions, the occurrence of infragravity waves having frequencies of 0.018–0.019 Hz was documented from swash measurements. The nearshore bars were located at theoretical antinode positions. On the basis of the longshore swash structure and the longshore rhythmic topography, the infragravity waves were hypothesized to be standing edge waves having three zero-crossings (n = 3) with the frequency being determined by a topographically induced cut-off mechanism (HUNTLEY, 1976). Here, surf zone measurements of a wave having a similar frequency have shown that the cross-shore structure was correlated with bar positions. However, the infragravity wave type cannot be documented conclusively, as we have no data on the longshore infragravity wave structure, and the manometer array was too close to shore to distinguish between edge waves and leaky modes—the structures of which are almost coincident close to the shoreline. Further, even though an electromagnetic current meter was deployed at T5, phase relations between currents and surface elevation cannot be computed due to the phase changes induced in the manometer tubes.

On the other hand, under standing edge waves and progressive incident waves, cross-shore and longshore currents (u–v) are in phase (0° or 180°), whereas these velocity components are in quadrature (90° or 270°) under progressive edge waves and leaky mode standing waves (*e.g.*, HUNTLEY and BOWEN, 1978). Table 2 shows phases at 0.018 Hz, computed from cross-spectral analysis of u and v at T5. At times when there was a significant coherence between u and v (approximately corresponding to the cases where the 0.018 Hz wave was statistically significant in the manometer records, see Table 1), phases were close to 0° or 180°. The 0.018 Hz wave was shown to possess a cross-shore standing structure, and the possibility of a progressive incident wave can be ruled out. Therefore, indications are that this wave (at least from 0400–1000 hr) was a standing edge wave.

At noon on November 18 (subsequent to the

storm), the second bar was rhythmic. The bar horns were very close to the mean water level and thus waves were breaking at these positions. The distance between bar horns was approximately 250 m. If bar rhythms are generated by a standing edge wave, the rhythmic wavelength, λ, can be computed from the edge wave dispersion relation

$$\lambda = L_e/2 = (g/4\pi)T_e^2 \sin(2n + 1)\beta \quad (10)$$

(URSELL, 1952), where L_e, T_e are the edge wave wavelength and period, respectively. On a slope of $\beta = 0.0150$, a 0.018 Hz standing edge wave would generate rhythmic wavelengths of 181 m (n = 2), 253 m (n = 3), or 325 m (n = 4). The mode 3 response is in good correspondence with the measured topography, and it is thus possible that the infragravity wave was in fact a mode 3 standing edge wave.

The standing infragravity wave identified in this experiment was only present for a relatively short period of time between 0200 hr and 1000 hr (Table 1). Its occurrence was coincident in time with the appearance of two incident wave spectral peaks which transferred energy to the infragravity wave through resonant triad interactions. As these two incident wave components became further separated in frequency space, the infragravity response vanished, albeit with some time lag (Figures 13 and 14; Table 1). It is of interest to speculate why only one standing infragravity wave was generated.

In an earlier study, AAGAARD (1990b) correlated an 0.018 Hz infragravity wave with a cut-off mode edge wave. According to the cut-off model (HUNTLEY, 1976), edge waves whose cross-shore length scale fit the dimensions (width and gradient) of the nearshore profile are preferentially selected and amplified. The edge wave cut-off period is given by

$$T_c = 2\pi(x_s/(g \tan \beta/3.5n(n + 1))^{1/2} \quad (11)$$

where n is the edge wave mode number and x_s is the width of the surf zone, measured from the shoreline to the slope break which is located at x $\approx$ 575 m at this location (Figure 2), corresponding to $x_s \approx$ 552 m at the storm peak. Equation 11 shows that for a given profile geometry, cut-off periods decrease with increasing mode number. In this particular case, a cut-off mode n = 3 edge wave would have a frequency of $\approx$0.0169 Hz which is close to the recorded frequency peak at 0.018 Hz.

Due to the lack of data from the outer parts of the profile, the validity of the cut-off model cannot be further substantiated here. The available data do suggest that the 0.018 Hz wave identified in the present study could have been an n = 3 standing edge wave. Whether it was indeed a cut-off wave cannot be established. If that was the case, it is remarkable that other cut-off modes were not generated and/or were not very strong. (In Figure 11a, coherence peaks at 0.011 Hz, and occasionally very small, statistically insignificant peaks were seen in the spectra at a similar frequency, *e.g.*, T4 in Figure 9. This frequency is close to the predicted n = 2 cut-off at 0.012 Hz.) It was hypothesized above that the 0.018 Hz response occurred when the incident wave band had a favourable spectral composition. The question is why other cut-off modes were not generated/amplified when the incident wave band was unsuitable for the generation of an n = 3 wave. For example, after 1000 hr, the incident wave peaks were apparently separated too far in frequency space to generate the mode 3 wave through difference interactions. But it might have been possible to generate higher cut-off modes with higher frequencies (Equation 11). Similarly, at the time when only one incident wave peak existed (prior to 0200 hr; Table 1 and Figure 14), it might have been possible to generate lower cut-off modes through difference interactions within this single incident wave peak. Why this did not occur is open to question. A possible answer could be that the presence of three bars preconditioned the infragravity response, *i.e.*, resulted in the selection of an n = 3 edge wave. However, any solution to these problems must await further theoretical work.

ACKNOWLEDGEMENTS

This study was supported by the Danish Natural Science Research Council, grant no. 11-8164. Additional data analysis was conducted while the first author held an NSERC International Postdoctoral Fellowship at the Department of Geography, University of Toronto. We are sincerely grateful to P. Nielsen, University of Queensland, for assistance with the construction of the barometer and for helpful discussions, and to J.C. Doering, University of Manitoba, for providing us with the bispectral algorithm. Comments by Dr. R.G. Dean and an anonymous reviewer were greatly appreciated and improved the contents of this paper. Finally, thanks are due to Dennis Anthony who assisted with the diving under near-freezing

conditions and to J. Jønsson for redrawing the figures.

LITERATURE CITED

AAGAARD, T., 1988. A study on nearshore bar dynamics in a low-energy environment; Northern Zealand, Denmark. *Journal of Coastal Research,* 4, 115–128.

AAGAARD, T., 1990a. Swash oscillations on dissipative beaches—Implications for beach erosion. *Journal of Coastal Research,* Special Issue No. 9, 738–752.

AAGAARD, T., 1990b. Infragravity waves and nearshore bars in protected, storm-dominated coastal environments. *Marine Geology,* 94, 181–203.

AAGAARD, T. and HOLM, J., 1989. Digitization of wave run-up using video records. *Journal of Coastal Research,* 5, 547–551.

BAUER, B.O. and GREENWOOD, B., 1990. Modification of a linear bar-trough system by a standing edge wave. *Marine Geology,* 92, 177–204.

BEACH, R.A. and STERNBERG, R.W., 1988. Suspended sediment transport in the surf zone: Response to cross-shore infragravity wave motion. *Marine Geology,* 80, 61–79.

BEACH, R.A. and STERNBERG, R.W., 1991. Infragravity driven suspended sediment transport in the swash, inner and outer-surf zone. *Proceedings Coastal Sediments '91,* American Society of Civil Engineers, pp. 114–128.

BOWEN, A.J., 1980. Simple models of nearshore sedimentation; beach profiles and longshore bars. *In:* MCCANN, S.B. (ed.), *The Coastline of Canada,* Geological Survey of Canada, Paper 80-10, pp. 1–11.

BOWEN, A.J. and GUZA, R.T., 1978. Edge waves and surf beat. *Journal of Geophysical Research,* 83, 1913–1920.

CARTER, T.G.; LIU, P.L.F., and MEI, C.C., 1973. Mass transport by waves and offshore sand bedforms. *Journal Waterways, Harbors and Coastal Engineering Division,* American Society of Civil Engineers, 99, 165–184.

DALLY, W.R., 1987. Longshore bar formation—Surf beat or undertow? *Proceedings Coastal Sediments '87,* American Society of Civil Engineers, 71–86.

DAVIDSON-ARNOTT, R.G.D. and MCDONALD, R.A., 1989. Nearshore water motion and mean flows in a multiple parallel bar system. *Marine Geology,* 86, 321–338.

DOERING, J.C., 1988. Wave-wave Interactions in the Nearshore. Unpublished Ph.D. Thesis, Dalhousie University, 139p.

DOERING, J.C. and BOWEN, A.J., 1986. Shoaling surface gravity waves: A bispectral analysis. *Proceedings 20th Coastal Engineering Conference,* American Society of Civil Engineers, 150–162.

DOERING, J.C. and BOWEN, A.J., 1987. Fundamental interactions in the nearshore. *Proceedings Coastal Sediments '87,* American Society of Civil Engineers, 710–722.

ELGAR, S. and GUZA, R. T., 1985. Observations of bispectra of shoaling surface gravity waves. *Journal of Fluid Mechanics,* 161, 425–448.

ELGAR, S. and GUZA, R.T., 1986. Nonlinear model predictions of bispectra of shoaling surface gravity waves. *Journal of Fluid Mechanics,* 167, 1–18.

GALLAGHER, B., 1971. Generation of surf beat by nonlinear wave interactions. *Journal of Fluid Mechanics,* 49, 1–20.

GREENWOOD, B., 1986. Sediment balance and bar morphodynamics in a multiple bar system: Georgian Bay, Canada. *In:* GARDNER, V. (ed.), *International Geomorphology 1986,* Proceedings 1st International Conference on Geomorphology, pp. 1119–1143.

GREENWOOD, B. and HALE, P. B., 1980. Depth of activity, sediment flux and morphological change in a barred nearshore environment. *In:* MCCANN, S.B. (ed.), *The Coastline of Canada,* Geological Survey of Canada. Paper 80-10, pp. 89–109.

GREENWOOD, B. and OSBORNE, P.D., 1991. Equilibrium slopes and cross-shore velocity asymmetries in a storm-dominated, barred nearshore system. *Marine Geology,* 96, 211–235.

GUZA, R.T. and THORNTON, E.B., 1982. Swash oscillations on a natural beach. *Journal of Geophysical Research,* 87, 483–491.

GUZA, R.T. and THORNTON, E.B., 1985. Observations of surf beat. *Journal of Geophysical Research,* 90, 3161–3172.

HAUBRICH, R. A., 1965. Earth noises, 5 to 500 millicycles per second. *Journal of Geophysical Research,* 70, 1415–1427.

HOLMAN, R.A., 1981. Infragravity energy in the surf zone. *Journal of Geophysical Research,* 86, 6442–6450.

HOLMAN, R.A. and BOWEN, A.J., 1979. Edge waves on complex beach profiles. *Journal of Geophysical Research,* 84, 6339–6446.

HOLMAN, R.A. and BOWEN, A.J., 1982. Bars, bumps and holes: Models for the generation of complex beach topography. *Journal of Geophysical Research,* 87, 457–468.

HOLMAN, R.A. and BOWEN, A.J., 1984. Longshore structure of infragravity wave motions. *Journal of Geophysical Research,* 89, 6446–6452.

HUNTLEY, D.A., 1976. Long-period waves on a natural beach. *Journal of Geophysical Research,* 81, 6441–6449.

HUNTLEY, D.A. and BOWEN, A.J., 1978. Beach cusps and edge waves. *Proceedings 16th Coastal Engineering Conference,* American Society of Civil Engineers, pp. 1378–1393.

KIM, Y.C. and POWERS, E.J., 1979. Digital bispectral analysis and its application to non-linear wave interactions. *IEEE Transactions on Plasma Science,* 1, 120–131.

LONGUET-HIGGINS, M.S. and STEWART, R.W., 1962. Radiation stress and mass transport in gravity waves, with application to surf beats. *Journal of Fluid Mechanics,* 13, 481–504.

NIELSEN, P., 1988. Wave set-up: A field study. *Journal of Geophysical Research,* 93, 15643–15652.

NIELSEN, P.; DAVIS, G.A.; WINTERBOURNE, J.M., and ELIAS, G., 1988. Wave Setup and the Water Table in Sandy Beaches. Public Works Department of New South Wales, Coastal Branch. Technical Memorandum TM 88/1, 132p.

OLTMAN-SHAY, J. and GUZA, R.T., 1987. Infragravity edge wave observations on two California beaches. *Journal of Physical Oceanography,* 17, 644–663.

RUSSELL, P.; DAVIDSON, M.; HUNTLEY, D.A.; CRAMP, A.; HARDISTY, J., and LLOYD, G., 1991. The British Beach

and Nearshore Dynamics (B-BAND) Programme. *Proceedings Coastal Sediments '91,* American Society of Civil Engineers, pp. 371–384.

SALLENGER, A.H. and HOLMAN, R.A., 1987. Infragravity waves over a natural barred profile. *Journal of Geophysical Research,* 92, 9531–9540.

SHORT, A.D., 1975. Multiple offshore bars and standing waves. *Journal of Geophysical Research,* 80, 3838–3840.

SVENDSEN, I.A., 1984. Mass flux and undertow in a surf zone. *Coastal Engineering,* 8, 347–365.

URSELL, F., 1952. Edge waves on a sloping beach. *Proceedings Royal Society of London,* A 214, pp. 79–97.